A&A 503, 639–650 (2009)
DOI: 10.1051/0004-6361/200810699

Astronomy & Astrophysics

A low-resolution near-infrared spectral library of M-, L-, and T-dwarfs⋆

L. Testi[1,2]

[1] INAF – Osservatorio Astrofisico di Arcetri, Largo E. Fermi 5, 50125 Firenze, Italy
e-mail: ltesti@eso.org
[2] European Southern Observatory, Karl Schwarzschild str. 2, 85748 Garching, Germany

Received 28 July 2008 / Accepted 6 April 2009

ABSTRACT

We present complete near-infrared (0.85–2.45 μm), low-resolution ($R \sim 100$) spectra of a sample of 54 disk M-, L-, and T-dwarfs with reliable optical or near infrared spectral-type classification from the literature. The observations were obtained with a prism-based optical element, the Amici device, which provides a complete spectrum of the source on the detector. Our observations indicate that low-resolution near-infrared spectroscopy can be used to determine the spectral classification of late-type field dwarfs in a fast but accurate way. We derive a set of near-infrared spectral indices that are useful to the classification of field dwarfs not seriously affected by reddening. Finally, we show that the comparison of Amici spectra with model atmospheres allows us to obtain a reliable estimate of the dwarf effective temperatures.

Key words. stars: low-mass, brown dwarfs – stars: fundamental parameters – infrared: stars

1. Introduction

We have witnessed an extraordinary evolution in the field of very low-mass stars and brown dwarfs. From being purely hypothetical objects, in only a few years, they have become first a curious oddity, following the first discoveries (Nakajima et al. 1995; Rebolo et al. 1995), then an entirely new class of stellar objects that required the definition of two new spectral classes: L (Martín et al. 1999; Kirkpatrick et al. 1999) and T (Kirkpatrick et al. 1999; Burgasser et al. 2002a; Geballe et al. 2002).

Very low-mass stars and brown dwarfs emit radiation mostly in the far red of the optical spectrum and in the near-infrared. For this reason the most successful strategies for identifying these objects have been based on near-infrared sky surveys, such as 2MASS (Kirkpatrick et al. 1999, 2000; Burgasser et al. 2002a) and DENIS (Delfosse et al. 1997; Tinney et al. 1998), and the red optical data of the SDSS (Fan et al. 2000). All of these surveys combined provide relatively good sensitivity in the appropriate bands and very wide area coverage. These two factors have allowed a sizeable number of nearby L- and T-type objects to be discovered, despite their intrinsic low luminosity.

Optical spectroscopic classification of the L-type objects, although feasible, has proven to be difficult because of the large amount of telescopes time required (Martín et al. 1999; Kirkpatrick et al. 1999). For this reason, several authors have attempted to relate the optical classification schemes to those in the near-infrared (e.g., Reid et al. 2001; Testi et al. 2001, hereafter T01; Geballe et al.2002). For T-dwarfs, optical classification is impractical and only near-infrared classification schemes have been proposed (e.g., Burgasser et al. 2002a, 2003; Geballe et al. 2002; Cushing et al. 2005). Because of the higher brightnesses of objects in the near infrared, these classification schemes, especially those based on low-resolution spectroscopy have proven to be very efficient.

The possibility of deriving a consistent method for near-infrared spectroscopic classification of atmospheres with spectral types later than mid-M is also attractive in confirming and classifying young, very low-mass objects in star-forming regions. The combination of cool atmospheres and environment extinction prevents the use of optical classification schemes in many young star-forming regions. As an example, Natta et al. (2002) and Testi et al. (2002) used low-resolution near-infrared spectroscopic classification methods to classify embedded young brown dwarfs in the ρ-Ophiuchi star-forming region.

In this paper, we present the results of very low-resolution near-infrared observations of 54 field dwarfs with spectral types in the range M3 to T8. The goal of these observations is to show that very low-resolution near-infrared spectroscopy allows one to classify these objects accurately and, by comparison with model atmospheres, to derive a good estimate of the atmospheric effective temperature. This work represents the extension and completion of our earlier work on field L-type dwarfs (T01). Bouvier et al. (2008) applied our spectral library to the classification young T-dwarfs in the Hyades cluster.

The paper is organized as follows. In Sect. 2, we describe the sample selection criteria, in Sect. 3, the observation setup and, in Sect. 4, our near-infrared cool dwarfs spectral library. In Sect. 5, we discuss a set of spectral indices useful to spectral classification. In Sect. 6, a comparison with model atmospheres is presented along with the method used to derive effective temperatures. In Sect. 7, we summarize the main conclusions of this study.

⋆ All the spectra presented in this paper are only available in electronic form at the CDS via anonymous ftp to cdsarc.u-strasbg.fr (130.79.128.5) or via
http://cdsweb.u-strasbg.fr/cgi-bin/qcat?J/A+A/503/639

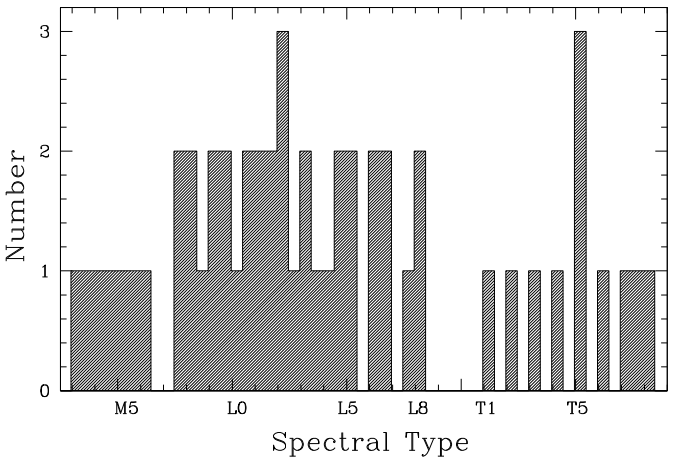

Fig. 1. Distribution of spectral types of the observed dwarfs.

2. The sample

Field dwarfs were selected in order to obtain a coverage of the spectral types from M3V to T8V as uniformly as possible. The M-dwarfs were selected from the samples of Henry et al. (1994) and Kirkpatrick et al. (1995, 1999) according to observability, magnitude, and spectral-type classification. The selection of the L-dwarf sample was described in T01. The T-dwarfs were selected from the samples of Burgasser et al. (2000, 2002a), Leggett et al. (2000), and Strauss et al. (1999). The final sample consists of 54 cool field dwarfs, 17 M type, 26 L type, and 11 T type.

Adopted from the literature, the spectral classification of the M- and L-dwarfs is based on optical, red spectroscopy, while the T-dwarf spectral types are based on the near-infrared classification scheme of Burgasser et al. (2004). These authors provided a new classification scheme that refines, solves inconsistencies, and supersedes the previous schemes in Burgasser et al. (2002a) and Geballe et al. (2002). The distribution of spectral types in our sample is shown in Fig. 1. We emphasize that some authors have identified inconsistencies between the optical and infrared classification schemes of late dwarfs (e.g., Geballe et al. 2002); we did not explore these differences in our work but rather related our spectral library to the optical classification (where available). As we show in the following sections, this approach is quite successful and we do not find evidence that the use of our infrared spectral library could lead to ambiguous classification.

We decided not to include the coolest objects discovered most recently (Warren et al. 2007; Delorme et al. 2008) as the spectral classification of these remains uncertain. The possibility of extending the spectral library to the coolest objects will be considered when a larger number of them will be available and an appropriate spectral sequence will have been defined.

3. Observations and data reduction

The observational data were collected at the 3.58 m TNG with the Near Infrared Camera and Spectrograph (NICS), a cryogenic focal reducer designed as a near-infrared common-user instrument for that telescope. The instrument is equipped with a Rockwell 1024^2 HAWAII near-infrared array detector. Among the many imaging and spectroscopic observing modes (Baffa et al. 2000, 2001), NICS offers a high throughput, very low-resolution mode with an approximately constant resolving power of ~50, when the 1″ wide slit is used. In this mode, a prism-based optical element, the Amici device, is used to obtain a complete 0.85–2.45 μm long-slit spectrum of the astronomical source on the detector (Baffa et al. 2001; Oliva 2003).

The M- and T-dwarfs in our sample were observed during several observing runs in the June 2001 to May 2003 period (see Table 1). We used the 0.5″ wide slit and the resulting spectra have an effective resolution of ~100 across the entire spectral range, similarly the L-dwarfs observations reported in T01. Integration times on source varied from a few to 25 min, depending on the source brightness and sky transparency conditions. Wavelength calibration was performed using an Argon lamp and deep telluric absorption features. The telluric absorption was then removed by dividing each of the object spectra by an A0 reference star spectrum observed at similar airmass; the reference star was generally drawn from the Arnica standards list (Hunt et al. 1998). Finally, flux normalization was completed using a theoretical A0 star spectrum smoothed to the appropriate resolution. No attempt was made to obtain an absolute flux calibration of the final spectra. All the spectra discussed in this paper were normalized to the average flux in the region 1.235–1.305 μm. The shapes of the final spectra were checked following the procedure outlined in T01. For all 11 T-dwarfs in our sample and 2 of the L-dwarfs in T01, low resolution, near-infrared spectra from IRTF/SpeX exist in the literature (Burgasser et al. 2004; Burgasser 2006; Cruz et al. 2004[1]). A comparison shows that the spectra from the two libraries are consistent within the uncertainties.

4. The Amici spectral library

The primary goal of this work was to provide a library of low-resolution near-infrared spectra of field dwarfs useful to spectral classification[2]. In Figs. 2 and 3 we show the spectra of M- and T-dwarfs, respectively; the L-dwarf spectra were shown already in T01 (their Fig. 1). Absorption features related to metals (KI, NaI) and molecules (TiO, FeH, CO) are visible in some of the spectra, depending on the spectral type and signal-to-noise ratio of the data, but are usually not resolved. The most prominent features in the spectra are those caused by water vapour and, for the coolest spectral types, methane absorption. These features, together with dust and H_2 collision induced absorption, determine the global shape of the spectra, which evolves distinctively from early M to late T types. These features and their theoretical interpretation have been discussed at length in the literature (Allard et al. 2001; Reid et al. 2001; Leggett et al. 2001; Burgasser et al. 2002a; Geballe et al. 2002; Tsuji 2002) and are not rediscussed here.

An important point for the study in this paper is that, even at this low spectral resolution, the spectra exhibit a smooth but distinctive variation as a function of spectral type. With the possible exception of a few spectra of the lower signal to noise ratio, the library of Amici field dwarf spectra can be used as a source of templates to derive spectral types for faint or embedded cool objects for which higher resolution infrared spectroscopy or optical spectroscopy is impractical. This method was applied with success in deriving spectral classifications of young embedded brown dwarfs (Natta et al. 2002; Testi et al. 2002; Bouvier et al. 2008).

[1] Available at `http://www.browndwarfs.org/spexprism`

[2] The complete Amici spectral library, including the data published in T01, is available at CDS, see footnote to the frontpage of this paper.

Table 1. Observed M-, L-, and T-dwarfs.

Name	α (2000)	δ (2000)	Sp. Type[a]	Obs. Date	Ref.[b]	Alternative Name	Notes
LHS 1439	02:44:15.5	+25:31:24	M3.0	12 Nov. 02	2	2MASS J02441537+2531249	
LHS 1723	05:01:57.4	−06:56:47	M3.5	25 Nov. 01	2	2MASS J05015746−0656459	
LHS 1047	00:15:28.1	−16:08:02	M4.0	12 Nov. 02	2	2MASS J00152799−1608008	
2MASSW J2300189+121024	23:00:18.9	+12:10:24	M4.5	03 Aug. 01	4	2MASS J23001886+1210238	
LP 766–89	01:00:49.1	−19:33:40	M5.0	12 Nov. 02	3	2MASS J01004911−1933398	
LP 759–25	22:05:35.7	−11:04:29	M5.5	12 Nov. 02	3	2MASS J22053575−1104287	
2MASSW J2308287+130928	23:08:28.7	+13:09:28	M6.0	03 Aug. 01	4		
LHS 2645	12:53:12.4	+40:34:04	M7.5	17 Jun. 01	3	2MASS J12531240+4034038	
2MASSW J2258066+154416	22:58:06.6	+15:44:16	M7.5	03 Aug. 01	4		
LP 412–31	03:20:59.7	+18:54:23	M8.0	03 Aug. 01	3	2MASS J03205965+1854233	
RG 0050−2722	00:52:54.7	−27:06:00	M8.0	03 Aug. 01	3	2MASS J00525468−2705597	
CTIO 0126575+280202	01:27:39.2	+28:05:54	M8.5	03 Aug. 01	3	2MASS J01273917+2805536	
TVLM 513−46546	15:01:08.2	+22:50:02	M8.5	17 Jun. 01	3	2MASS J15010818+2250020	
LHS 2065	08:53:36.2	−03:29:32	M9.0	25 Nov. 01	3	2MASS J08533619−0329321	
TVLM 868−110639	15:10:16.9	−02:41:08	M9.0	17 Jun. 01	3	2MASS J15101685−0241078	
PC 0025+0447	00:27:42.0	+05:03:41	M9.5	07 Jul. 01	3	2MASS J00274197+0503417	Young
2MASSW J0149090+295613	01:49:09.0	+29:56:13	M9.5	03 Aug. 01	4	2MASS J01490895+2956131	
2MASSW J0058425−065123	00:58:42.5	−06:51:24	L0.0	08 Dec. 00	5	2MASS J00584253−0651239	
2MASSI J0746425+200032	07:46:42.6	+20:00:32	L0.5	08 Dec. 00	5	2MASS J07464256+2000321	
2MASSW J1412244+163312	14:12:24.5	+16:33:12	L0.5	14 Jan. 01	5	2MASS J14122449+1633115	
2MASSW J0208183+254253	02:08:18.3	+25:42:53	L1.0	08 Dec. 00	5		
2MASSW J1035245+250745	10:35:24.5	+25:07:45	L1.0	14 Jan. 01	5		
2MASSW J0832045−012835	08:32:04.5	−01:28:36	L1.5	08 Dec. 00	5	2MASS J08320451−0128360	
2MASSW J1411175+393636	14:11:17.4	+39:36:36	L1.5	16 Jan. 01	5	2MASS J14111735+3936363	
2MASSW J0015447+351603	00:15:44.7	+35:16:03	L2.0	09 Dec. 00	5		
2MASSI J0753321+291711	07:53:32.2	+29:17:12	L2.0	12 Dec. 00	5	2MASS J07533217+2917119	
2MASSW J0829066+145622	08:29:06.6	+14:56:23	L2.0	08 Dec. 00	5	2MASS J08290664+1456225	
2MASSI J1029216+162652	10:29:21.7	+16:26:53	L2.5	08 Dec. 00	5	2MASS J10292165+1626526	
2MASSI J0302012+135814	03:02:01.2	+13:58:14	L3.0	11 Dec. 00	5	2MASS J03020122+1358142	
2MASSI J0409095+210439	04:09:09.5	+21:04:39	L3.0	13 Dec. 00	5	2MASS J04090950+2104393	
2MASSW J0036159+182110	00:36:16.2	+18:21:10	L3.5	03 Feb. 01	5	2MASS J00361617+1821104	
2MASSW J1246467+402715	12:46:46.8	+40:27:15	L4.0	16 Jan. 01	5	2MASS J12464678+4027150	
2MASSW J0740096+321203	07:40:09.7	+32:12:03	L4.5	12 Dec. 00	5	2MASS J07400966+3212032	
2MASSW J1112257+354813	11:12:25.7	+35:48:13	L4.5	13 Jan. 01	5	2MASS J11122567+3548131	binary
2MASSW J0208236+273740	02:08:23.6	+27:37:40	L5.0	15 Jan. 01	5	2MASS J02082363+2737400	
2MASSW J1239272+551537	12:39:27.3	+55:15:37	L5.0	14 Jan. 01	5	2MASS J12392727+5515371	binary
2MASSI J0103320+193536	01:03:32.0	+19:35:36	L6.0	04 Feb. 01	5	2MASS J01033203+1935361	
2MASSI J0756252+124456	07:56:25.2	+12:44:56	L6.0	12 Jan. 01	5	2MASS J07562529+1244560	
2MASSW J0829570+265510	08:29:57.1	+26:55:10	L6.5	08 Dec. 00	5	2MASS J08295707+2655099	
2MASSW J0920122+351742	09:20:12.2	+35:17:43	L6.5	14 Jan. 01	5	2MASS J09201223+3517429	binary
2MASSI J0825196+211552	08:25:19.7	+21:15:52	L7.5	12 Jan. 01	5	2MASS J08251968+2115521	
2MASSW J0310599+164816	03:10:59.9	+16:48:16	L8.0	14 Jan. 01	5		
2MASSW J1523226+301456	15:23:22.6	+30:14:56	L8.0	02 Feb. 01	5	2MASS J15232263+3014562	
SDSSp J083717.22−000018.3	08:37:17.2	−00:00:18	T1.0	08 May 03	1	SDSS J083717.22−000018.3	
SDSSp J125453.90−012247.4	12:54:53.9	−01:22:47	T2.0	17 Jun. 01	1	2MASS J12545393−0122474	
SDSSp J102109.69−030420.1	10:21:09.7	−03:04:20	T3.0	13 May 03	1	2MASS J10210969−0304197	binary
2MASSI J2254188+312349	22:54:18.9	+31:23:50	T4.0	22 Aug. 02	1	2MASS J22541892+3123498	
2MASSI J0755480+221218	07:55:48.0	+22:12:17	T5.0	25 Nov. 01	1	2MASS J07554795+2212169	
2MASSI J2339101+135230	23:39:10.3	+13:52:28	T5.0	22 Aug. 02	1	2MASS J23391025+1352284	
2MASSI J2356547−155310	23:56:54.8	−15:53:11	T5.0	22 Aug. 02	1	2MASS J23565477−1553111	
SDSSp J162414.37+002915.6	16:24:14.4	+00:29:16	T6.0	17 Jun. 01	1	2MASS J16241436+0029158	
2MASSI J0727182+171001	07:27:18.2	+17:10:01	T7.0	25 Nov. 01	1	2MASS J07271824+1710012	
Gliese 570D	14:57:15.0	−21:21:48	T7.5	17 Jun. 01	1	2MASS J14571496−2121477	
2MASSI J0415195−093506	04:15:19.5	−09:35:07	T8.0	25 Nov. 01	1	2MASS J04151954−0935066	

[a] For M- and L-dwarfs we list the optical spectral types (from the reference in Col. 4), for T-dwarfs we list the NIR spectral types (from Burgasser et al. 2004).
[b] 1: Burgasser et al. (2004); 2: Henry et al. (1994); 3: Kirkpatrick et al. (1995); 4: Kirkpatrick et al. (1999); 5: Kirkpatrick et al. (2000).

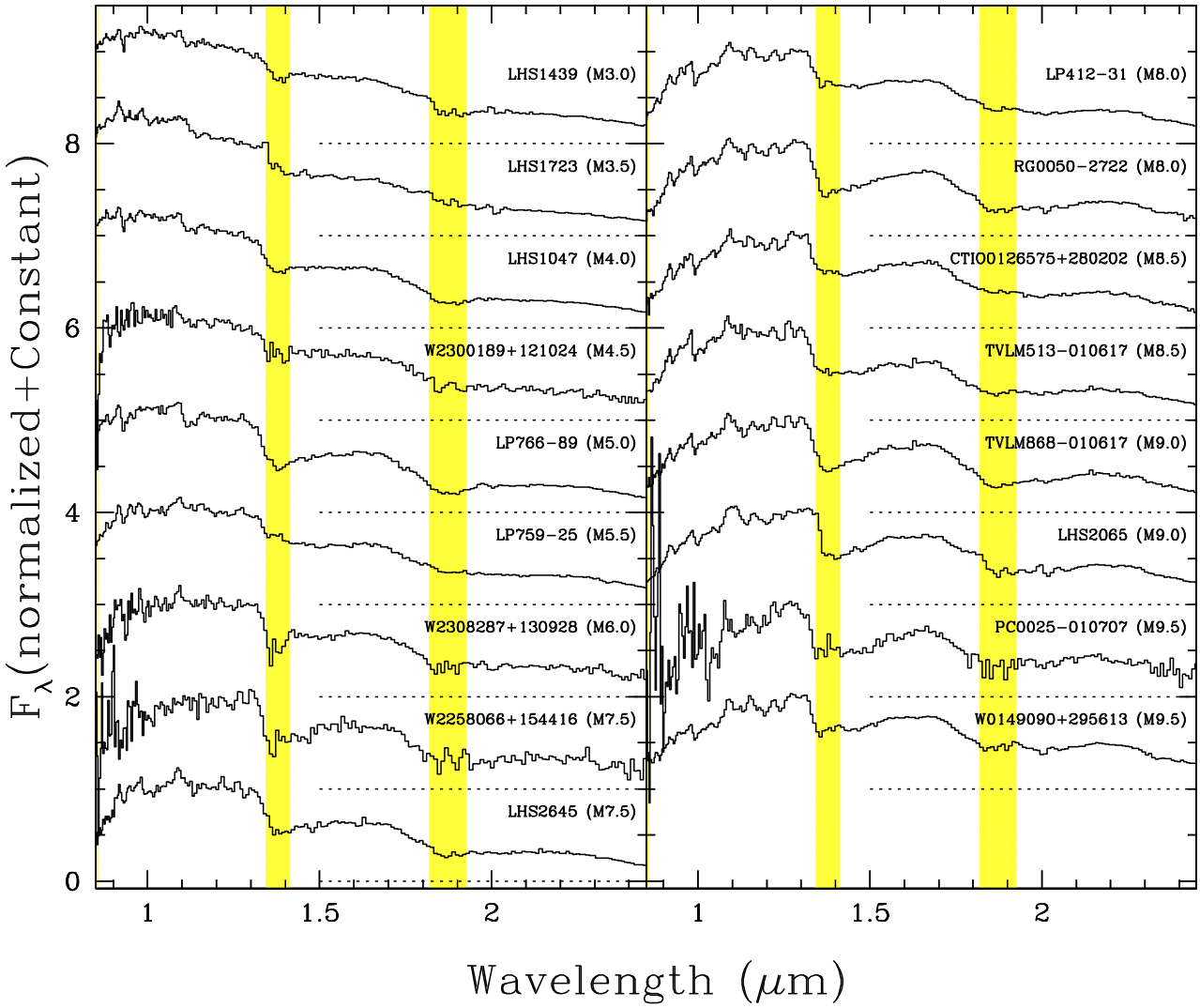

Fig. 2. NICS/Amici 0.85–2.45 μm low-resolution near-infrared spectra for all the M-Dwarfs in our sample. All spectra have been normalized by the average flux between 1.235 and 1.305 μm and a constant shift has been added to each to separate them vertically, the zero level for each spectrum is indicated by the dotted lines. Each spectrum is labeled with the name (for 2MASS objects the 2MASSJ prefix has been omitted) and the optical spectral type (see Table 1 for details). The shaded regions mark the spectral ranges where atmospheric absorption is most severe (between the *J* and *H* bands and between the *H* and *K* bands).

5. Spectral indices useful for classification

It is more practical to use a set of spectral indices when determining an approximate spectral classification. Many authors have proposed various near-infrared spectral indices that are useful in classifying of M-, L- and T-dwarfs (Reid et al. 2001; Burgasser et al. 2002a; Geballe et al. 2002). In T01, we discussed a set of indices based on our low-resolution near-infrared spectra that measure the slope of the residual continuum and the strength and shape of the main water vapour absorption bands. The numerical values of these indices for to our original sample of L-dwarfs, showed a tight correlation with the optically determined spectral types.

In Figs. 4 and 5, we show the values of the "continuum" (sHJ and sKJ) and water-band indices (sH_2O^J, sH_2O^{H1}, sH_2O^{H2}, sH_2O^K) defined in T01 as a function of spectral type for our complete sample of M-, L-, and T-dwarfs.

Both indices measuring the continuum slope (Fig. 4) show a tight correlation from the early M to the late L types corresponding to a progressive reddening of the spectrum. This trend is abruptly reversed for the T-dwarfs, which exhibit a strong blueing of the indices. This is caused by methane absorption and dust distribution in the atmosphere (see Allard et al. 2001). Methane absorption mainly affects the peak of the *H* and *K* bands, and our indices measure the depth of the methane absorption more than the continuum spectral slope of T-dwarfs. A similar trend is also evident for the broad-band colors (Kirkpatrick et al. 1999, 2000; Burgasser et al. 2002a),where the progressive reddening from early M to late L types is reversed for the T-dwarfs.

The water indices (Fig. 5) are very well correlated with spectral type from the early M to the late L dwarfs. With the exception of the sH_2O^J index, the other indices show a less tight correlation with spectral type in the T-dwarf range, mainly because of the competing effect of the methane absorption.

As discussed by Burgasser et al. (2002a) and Geballe et al. (2002), the classification of T-dwarfs is based on the spectral features produced by the methane absorption. It is thus clear that the most useful spectral classification indices are related to the methane features. The success of the sH_2O^J index in classifying T-dwarfs is due to its sensitivity to the methane

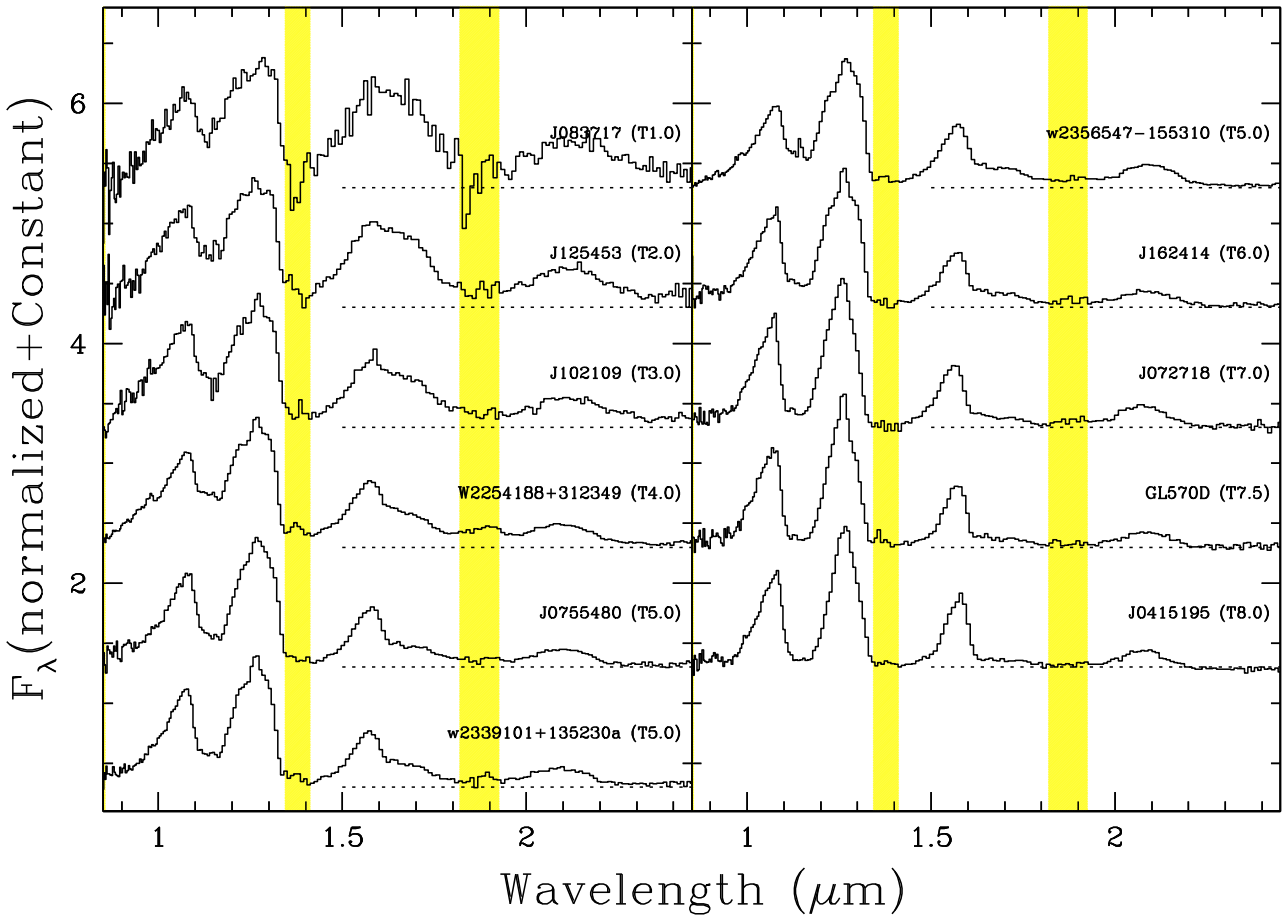

Fig. 3. Same as Fig. 2 (2MASS and SDSS names have been abbreviated). The spectral types are from Burgasser et al. (2002a).

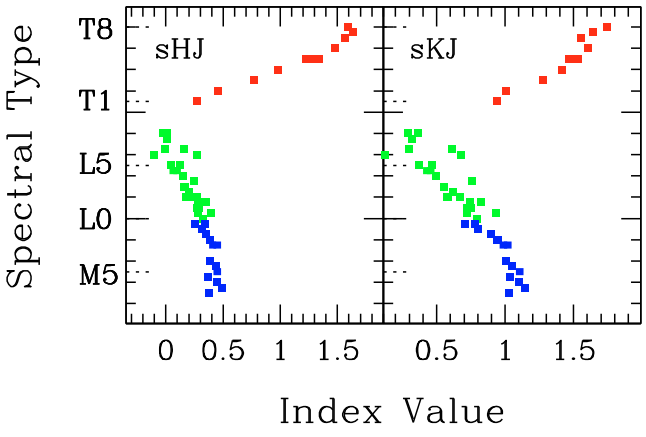

Fig. 4. Continuum-slope spectral indices, see T01 for the definition. Note that the indices indicate a progressive reddening of the continuum from the early M to the late L types, and a sharp blueing for T-dwarfs (see details in the text).

feature, which is very close to the water band at 1.15 μm. We do not define new methane indices for the spectral classification of T-dwarfs, but instead show in Fig. 6 the value of the indices defined by Burgasser et al. (2002a) computed using our spectra. The values and correlation with spectral types are similar to the results of Burgasser et al. and we emphasize here that these same indices can be used to classify T-dwarfs using NICS/Amici spectra.

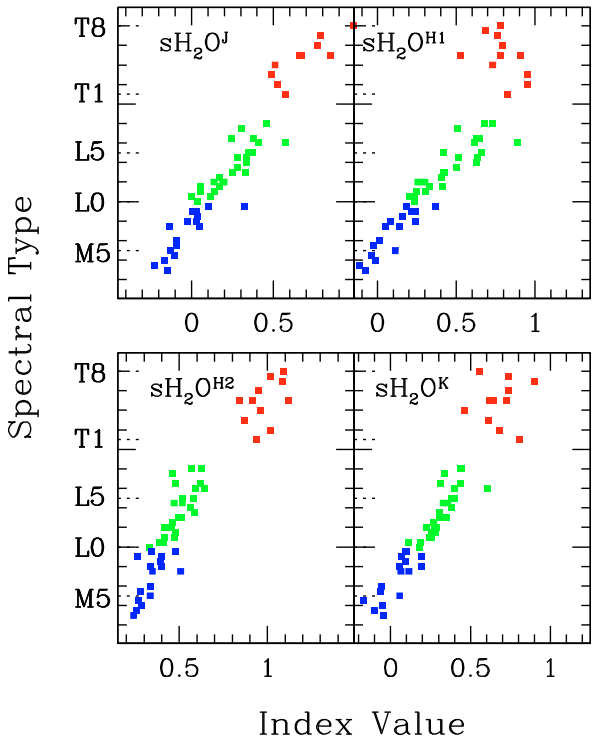

Fig. 5. Water bands spectral indices, see T01 for the definition. The indices sH_2O^{H1}, sH_2O^{H2}, and to some extent sH_2O^K do not show a tight correlation with T spectral types because of the effect of methane absorption.

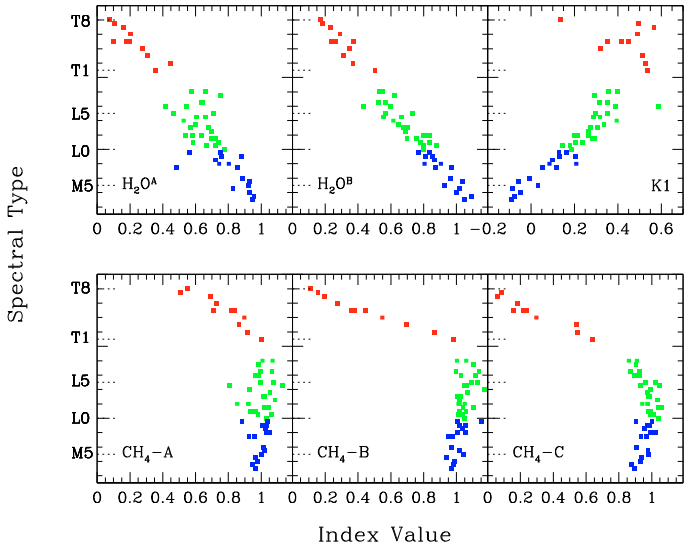

Fig. 6. Run of the H_2O^A, H_2O^B, K1, CH_4–A, CH_4–B, and CH_4–C indices as a function of spectral type, see Reid et al. (2001), Tokunaga & Kobayashi (1999), and Burgasser et al. (2002a) for the definitions.

In Appendix A, we present an example of using two of the most reliable indices for the spectral classification of field dwarfs. Even if the method that we describe is reasonably accurate for many applications, we emphasize that spectral classification is most reliably achieved by comparing the complete spectra of the objects to be classified with the spectra of objects of known spectral type in the library.

5.1. Classification of reddened late-type objects

Low-resolution near-infrared spectroscopy is especially useful to the spectral classification of embedded cool objects, such as young brown dwarfs in star-forming regions (e.g., Testi et al. 2002; Natta et al. 2002). Other authors have discussed the issue of using dwarfs (or luminosity class V) as spectral standards for young pre-main-sequence objects (which have spectral properties of subgiants, or luminosity class IV). Wilking et al. (2003) showed that the spectral index they define for the classification of young M-type brown dwarfs has values closer to those of dwarfs rather than to giants (or luminosity class III). Other authors have highlighted the differences between young objects, field dwarfs, and giants (e.g., Kirkpatrick et al. 2006; Allers et al. 2007), A discussion of this problem is beyond the scope of this paper; we note, however, that, despite the difference in surface gravity, field M- and L-type dwarfs can be used, and indeed have been used, as comparison standards in classifying young embedded very low-mass stars and brown dwarfs (Natta et al. 2002; Testi et al. 2002). The computation of the spectral indices in the previous section for young objects in the SpeX Prism library are indeed consistent with their published spectral types (see Appendix A).

The use of spectral indices as defined in the previous section may be inpractical for reddened objects (see Appendix A). This is because, indices that measure the spectral slope at two wavelengths are systematically affected by extinction and any error in the dereddening of the spectra will be directly reflected in an error in the estimated spectral type.

To circumvent this uncertainty, Wilking et al. (1999) defined a spectral index, called Q, which measures the strength of the water absorption bands within the NIR K-band; it is formally insensitive to extinction and exhibits a very good correlation with M subtypes. In this paper, we call this index Q_K. The use of this index with our Amici spectra is inpractical because it samples regions of the spectrum close to 2.5 μm that are usually affected by very high background, detector non-linearity, and low signal-to-noise ratio (in our Amici setup at the NICS/TNG). Additionally, the effectiveness of the Q_K index is significantly reduced once the methane absorption become important and suppresses the peak emission in the K-band.

A similar index was defined by Lucas et al. (2001) for the H-band, which we call Q_H. This index shows a strong correlation between the M and mid-L types and for the late T-types where the methane absorption features in the H-band are more prominent. Its effectiveness is lower between the mid-L and mid-T range, where the correlation with spectral types is not so strong (see Fig. 7).

We explored the possibility of defining new indices at J, H, and K band that are generally insensitive to errors in the determination of extinction and subsequent dereddening of the observed spectra. None of the indices that we define is as strictly reddening-independent as the Q_H and Q_K indices defined by Lucas et al. (2001) and Wilking et al. (1999), so all of them require an estimate of the reddening and a dereddening of the spectrum before the computation of the index and the estimate of the resulting spectral type. The indices are defined as:

$$I_J = \frac{\langle F_{1.09-1.13}\rangle + \langle F_{1.33-1.35}\rangle}{2 \times \langle F_{1.265-1.305}\rangle} \quad (1)$$

$$I_H = \frac{\langle F_{1.44-1.48}\rangle + \langle F_{1.76-1.80}\rangle}{2 \times \langle F_{1.56-1.60}\rangle} \quad (2)$$

$$I_K = \frac{\langle F_{1.96-1.99}\rangle + \langle F_{2.35-2.39}\rangle}{2 \times \langle F_{2.12-2.16}\rangle} \quad (3)$$

where, as in T01, $\langle F_{\lambda_i-\lambda_j}\rangle$ is the average flux measured in the range λ_i to λ_j. The variation in all of these indices, including Q_H and Q_K, with the spectral type of the observed field dwarfs is shown in Fig. 7. To explore the effects of an incorrect reddening correction, we simulated a dereddening error of plus and minus 3 mag (using the Cardelli et al. 1989, extinction law) and recomputed the indices. The results are shown as black crosses in the same Fig. 7. As expected, these reddening errors do not seriously compromise the classification using the I_H, I_K, and especially the Q_H and Q_K indices. The I_J index, however, is more sensitive to dereddening errors and the relatively large errors that we simulated would compromise the classification by several subtypes. An example of the results that can be expected when classifying reddened objects using the reddening independent indices is given in Appendix A.

6. Comparison with model atmospheres

Ultimately, the goal of the spectral classification of an observed object is to estimate its atmospheric physical parameters, mainly the effective temperature, surface gravity, and metallicity. Burgasser et al. (2004) showed metallicity differences in low-resolution infrared spectra of late dwarfs, although detailed empirical calibrations and extensive grids of model atmospheres of different metallities are still lacking, we therefore chose not to explore the effects of metallicity in this paper. The comparison of our low-resolution spectra with model libraries allows us to obtain meaningful estimates of effective temperature and surface gravity. To explore this possibility, we devised a procedure

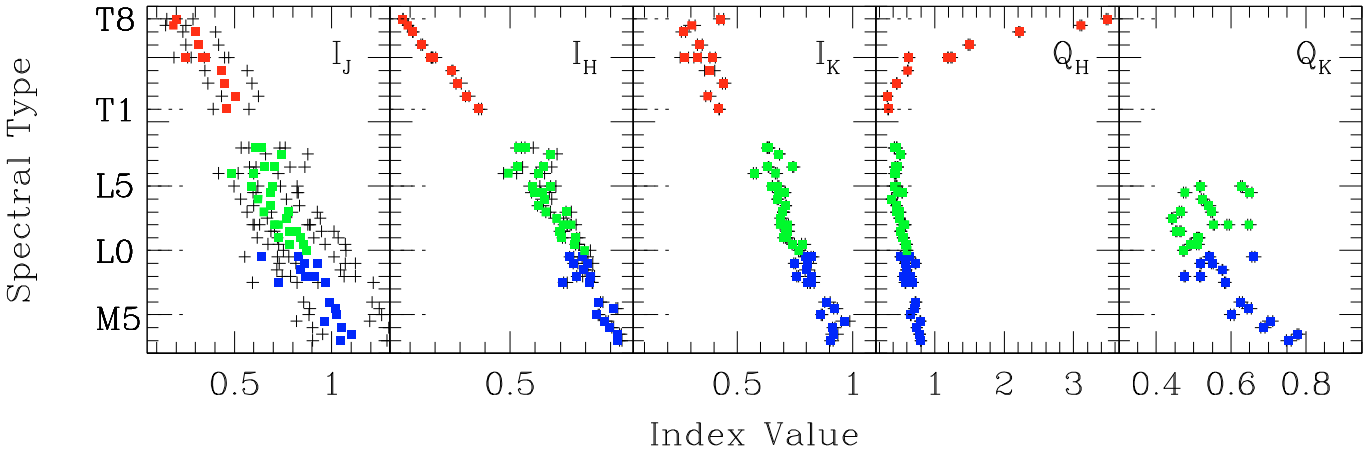

Fig. 7. Run of the I_J, I_H, and I_K indices as a function of spectral type. Filled squares show the indices values for a correct dereddening of the dwarf spectra; for each spectrum, the crosses represent the value of the index assuming a dereddening with an error of ±3 mag in A_V. In the rightmost two panels, we also show the run of the Q_H and Q_K indices.

for fitting theoretical model spectra to our Amici spectra. The model grids used in this exercise are those of the Lyon group (Allard et al. 2001). The models span a wide range of effective temperatures and surface gravities for solar metallicities and a set of assumptions about both the dust location in the atmosphere and various types of molecular opacities. In our fits, we used three classes of models: the Dusty, Settl, and Cond models with AMES molecular opacities (see Allard et al. 2001; Leggett et al. 2001, 2002, for details on the models).

The atmosphere model fits to the observed spectra were performed following a procedure similar to that of Leggett et al. (2002). For a given observed spectrum, the model spectra were smoothed to the appropriate resolution using a Gaussian function kernel and resampled on the same wavelength grid as the observational data; the model data were then scaled to the average flux of the observed spectrum and two merit figures were computed: the "q-estimator" defined by Leggett et al. (2002), and a classical χ^2. For each observed spectrum, we extracted the model spectra with the minimum value of "q" and χ^2; in general, with a few exceptions, the two best-fit models are either the same or have very similar physical parameters. To avoid problems with low signal-to-noise ratios and/or poor telluric correction, only spectral regions outside the worse telluric absorption windows were used for all the steps described above. This procedure was followed for the three class of models considered: Dusty, Settl, and Cond.

The results of the three classes of atmospheric model fits were inspected for each object. With some individual exceptions, the general trend was consistent with the expectations: the Dusty models offer more reliable fits than the other classes, for M-type and early L-type dwarfs; the Settl models appear to be the most appropriate for late L-type and early T-type dwarfs; while the late type T-dwarf spectra are best fit by Cond models. We defined the ranges of applicability of the three classes of models as follows: Dusty for M to L4 dwarfs, Settl for L5 through T2, and Cond for T3 through T8. These boundaries were chosen in an arbitrary way, the different classes of models usually providing equivalent fits to the transition types. Some examples of the fit results are shown in Appendix B along with a table of the best-fit model parameters derived from the two methods.

In Fig. 8, we show the variation in the effective temperature of the best-fit models as a function of the spectral type of the observed dwarf. We find a generally good correlation and conclude that our model fitting procedure can be used to estimate the effective temperature of the observed dwarfs with an uncertainty of ~100–150 K. This, of course, neglects any possible systematic model uncertainties.

In Fig. 8, we also show the results of our studies for the L-dwarf range only (Marley et al. 2002; Burgasser 2001) and down to the T-dwarf regime (Nakajima et al. 2004). All of these authors derived the effective temperatures based on objects with known parallaxes and by applying appropriate bolometric corrections to the measured magnitudes, and derived the effective temperatures from the bolometric luminosities and expected radius. It is comforting to verify that by fitting model atmospheres to the observed spectra, we derive values that are in reasonable agreement with these estimates. There are some possible systematic differences around the early and, more noticeably, late L types. The effective temperatures that we derive for the late L objects appear to be systematically ~200 K above the other estimates. We note that the L to T transition region is critical to the models; in this range, it is indeed expected that the formation and vertical location of dust clouds in the atmosphere will drastically affect the emerging near-infrared spectrum (see e.g., the discussion in Ackerman & Marley 2001; Burgasser et al. 2002b; and in Tsuji et al. 2004). It is clear that to obtain a satisfactory description of the atmospheres for these spectral types, the models need to take into account the complicated physics of cloud formation and stratification (see e.g., Tsuji et al. 2004).

The surface gravity is far less tightly constrained by these types of fits than to the effective temperatures. Our best-fit model parameters are within the ranges expected for old field dwarfs (mostly $5.0 \leq \log(g) \leq 6.0$, in cgs units). Significant differences in the fits are expected for much lower gravity objects, such as young very low-mass stars in star-forming regions or late-type Giants.

Even if our results are very consistent with other studies, we note that our derivation of the photospheric parameters are also affected by the uncertainties in the model atmospheres that we have used. As an example, using different atmosphere models, Cushing et al. (2008) derived photospheric temperatures for two of the T-dwarfs in our sample that are significantly lower (~300 K) than our estimates (and also lower than the Golimowski et al. 2004, fit).

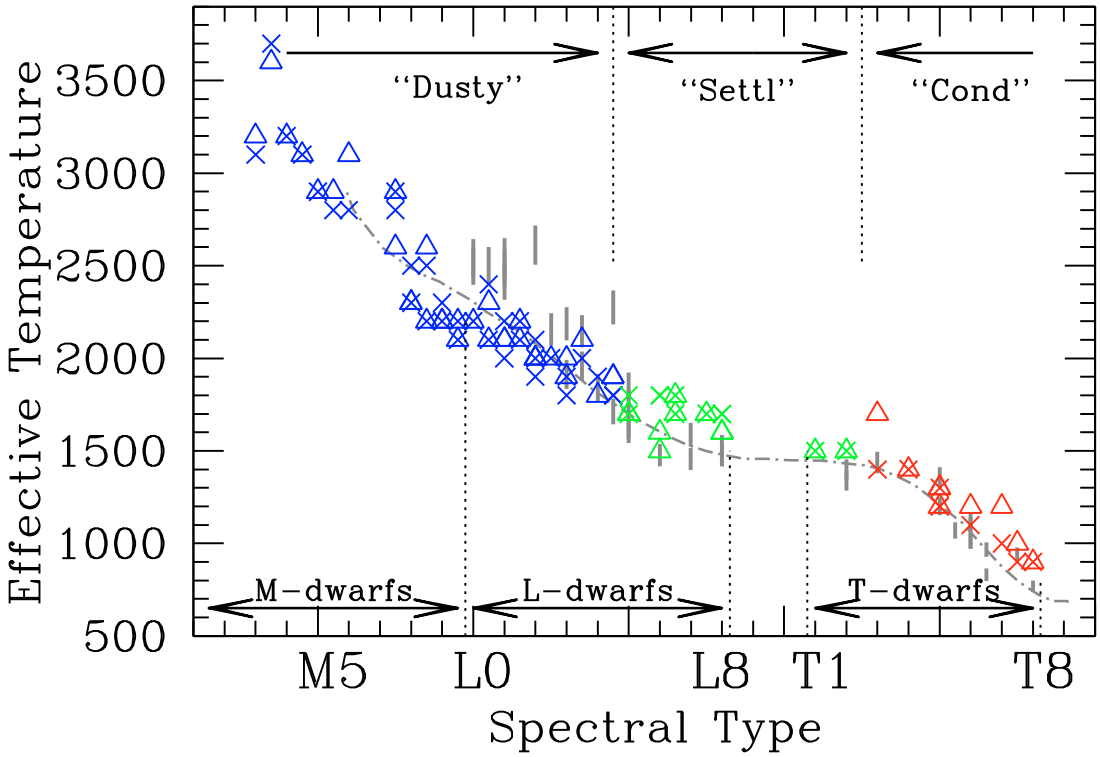

Fig. 8. Effective temperature of the best-fit atmospheric model as a function of spectral type. The triangles are obtained using the "q-estimator" fitting method (Leggett et al. 2002), while the crosses are the results of a standard χ^2 minimization. Different classes of atmospheric models have been used in different spectral type ranges, as indicated in the upper part of the figure. See text for details. For comparison we show the empirical results based on broad-band photometry of Golimowski et al. (2004, dot-dashed line) and the modeling results from Nakajima et al. (2004, vertical bars).

7. Conclusions

We have presented a library of very low resolution, complete near-infrared spectra of M-, L-, and T-dwarfs in the solar neighborhood. We have confirmed and extended our earlier suggestions that low-resolution near-infrared spectroscopy is a powerful method for confirming and classifying faint dwarfs.

We have proposed a set of spectral indices that can be used to perform an accurate classification of faint dwarfs based on low-resolution spectra. Some of these indices are defined in such a way as to mitigate the effects of an incorrect or incomplete correction of the observed spectra for the effects of interstellar extinction.

The results of theoretical model atmosphere fits to our observed spectra have shown that the comparison between models and observations at this spectral resolution allows us to derive a reasonably accurate estimate of the effective temperature of the photospere. The values of the surface gravity derived from these model fits are within the expectations for old field dwarfs. Quantitative comparison with lower gravity objects is required to assess whether very low resolution spectra allow this additional atmospheric parameter to be constrained.

Acknowledgements. I would like to acknowledge early contributions to this work from F. Ghinassi, J. Licandro, A. Magazzù, A. Natta, E. Oliva, F. D'Antona, C. Baffa, G. Comoretto, S. Gennari, and F. Lisi. I also thank F. Allard for allowing the use of the cool dwarf atmosphere model spectra. This research has benefitted from the SpeX Prism Spectral Libraries, maintained by Adam Burgasser at `http://www.browndwarfs.org/spexprism`. This work has been partly supported by the MIUR grant 2002028843_001. Support from ASI grants ARS-99-15 and 1/R/27/00 to the Osservatorio di Arcetri is also gratefully acknowledged. It is a pleasure to thank the Arcetri and TNG technical staff and the TNG operators for their assistance during NICS commissioning and observing runs.

Appendix A: Example of spectral classification using the spectral indices

In this Appendix, we describe a possible pplicationof the spectral indices we have investigated in this paper in classifying cool photospheres. We note that spectral classification is by definition a process of classifying photospheres using global spectral properties. The use of spectral indices can only provide an approximate estimate of the spectral class of a given object and whenever possible a classification based on a direct comparison of the full spectrum with template spectra (such as those provided in our spectral library) should be used.

As an illustration, we use the indices sH_2O^J and sHJ to estimate the spectral types of the field dwarfs in the SpeX Prism library[3]. The procedure that we used is the following. We first estimated the spectral type using the water index: if the derived spectral type was in the M- or L-type range this provided directly the estimated spectral type of the object; if the estimated type was in the T-type range, we used the sHJ index to estimate the spectral type. In both cases to perform the spectral type estimate, we used quadratic fits to the datapoints in our Amici spectral library (i.e., the points shown in Figs. 4 and 5).

In Fig. A.1, we show the results of this procedure for the SpeX spectra of field M-, L-, and T-dwarfs. The procedure is able to assign a spectral type that is accurate to within one subclass for the majority of objects. No systematic offset or error is evident, even though very few objects show a discrepancy of more than two subclasses.

[3] `http://www.browndwarfs.org/spexprism`

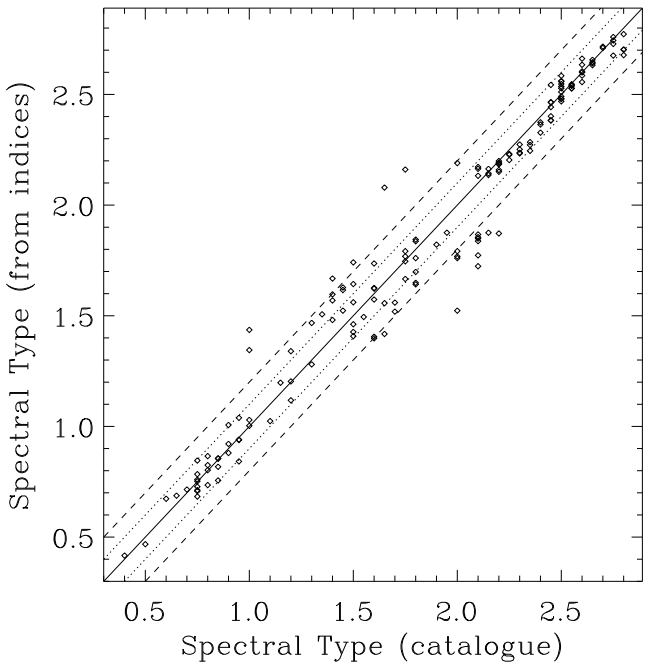

Fig. A.1. Spectral types estimated using the spectral indices (see text) compared with the catalogued spectral index for the SpeX spectra of field dwarfs. The solid line marks the locus of identical types, the dotted and dashed lines show interval representing differences of ±one and two subclasses, respectively. In this and the following figures in this Appendix (and in all the associated computations) we have coded the spectral types as: M0 = 0.0, M1 = 0.1, ..., L0 = 1.0, ..., T8 = 2.8.

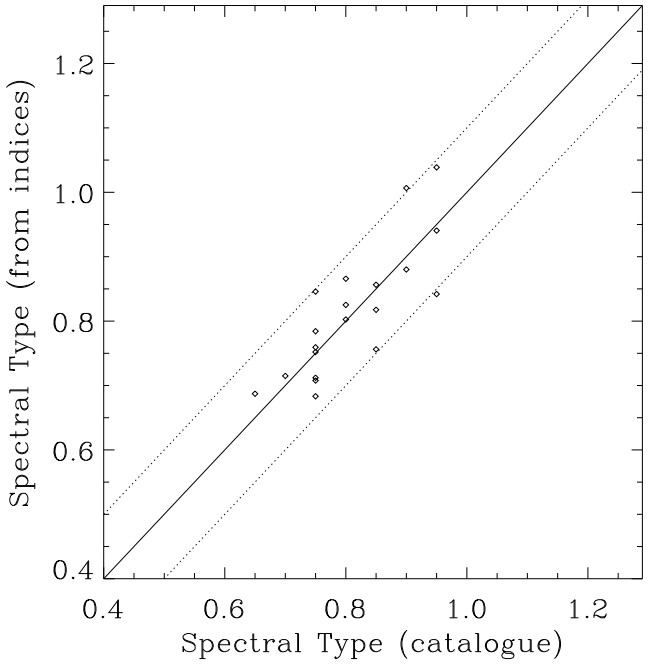

Fig. A.2. As Fig. A.1 but for young braown dwarfs in star forming regions. Note the different range in spectral types, which in this case only cover the range M6–M9.

We have also tested the procedure for the SpeX spectra of young objects (see Fig. A.2), which are all in the very narrow range M6–M9. The classification using the spectral index is remarkably accurate with all the objects classified being within one spectral subclass of their assigned spectral type.

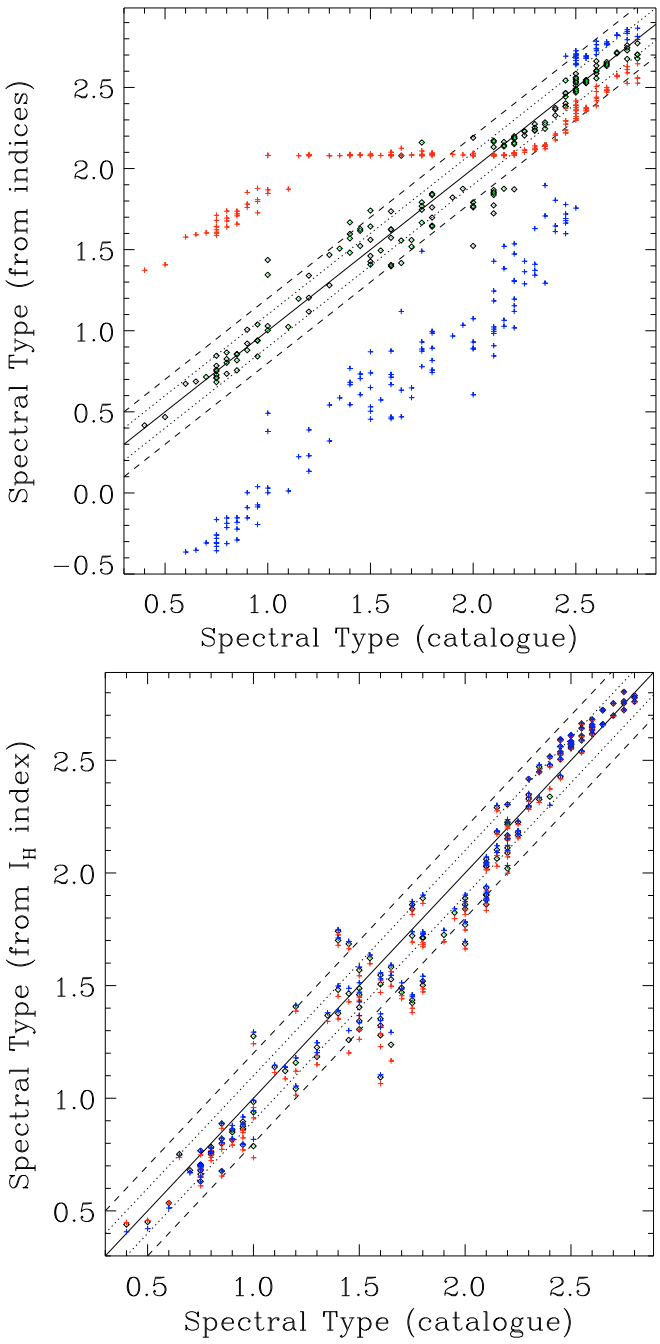

Fig. A.3. *Top panel*: as Fig. A.1 with added the derived spectral types assuming a dereddening error of $A_V = -5$ mag (blue crosses) and $A_V = 5$ mag (red crosses). *Bottom panel*: same as upper panel but the spectral types have been estimated using the I_H reddening independent index.

As noted in Sect. 5 of the main text, the values of the spectral indices are affected by extinction. To illustrate the effect of an incorrect correction for the extinction on the estimated spectral types, we performed the same computation as above for the SpeX dwarfs spectra but assuming an error in dereddening of $A_V \pm 5$ mag (and assuming the Cardelli et al. 1989, extinction law). The results, shown in Fig. A.3 top panel, show that the error introduced into the estimate of the spectral type is very large, making the use of the spectral indices essentially useless. In contrast, if the estimate of the spectral type is made using a quadratic fit to the reddening independent index I_H (as derived from our Amici spectral library), the effect of the erroneous correction for

Table B.1. Model atmospheres fitting results. For each object we provide the effective temperature and the surface gravity of the best fitting model with the χ^2 and the q methods (see text).

		DUSTY χ^2		DUSTY q		SETTL χ^2		SETTL q		COND χ^2		COND q	
Name	Sp.T.	$T_{\rm eff}$	Log(g)	$T_{\rm eff}$	Log(g)	$T_{\rm eff}$	Log(g)	$T_{\rm eff}$	Log(g)	$T_{\rm eff}$	Log(g)	$T_{\rm eff}$	Log(g)
LHS 1439	M3.0	3100	5.0	3200	5.0	–	–	–	–	–	–	–	–
LHS 1723	M3.5	3700	6.0	3600	6.0	–	–	–	–	–	–	–	–
LHS 1047	M4.0	3200	5.0	3200	5.0	–	–	–	–	–	–	–	–
2MASSW J2300189+121024	M4.5	3100	5.0	3100	5.0	–	–	–	–	–	–	–	–
LP 766–89	M5.0	2900	4.5	2900	4.5	–	–	–	–	–	–	–	–
LP 759–25	M5.5	2800	5.0	2900	5.0	–	–	–	–	–	–	–	–
2MASSW J2308287+130928	M6.0	2800	5.0	3100	5.0	–	–	–	–	–	–	–	–
LHS 2645	M7.5	2900	5.0	2900	5.0	–	–	–	–	–	–	–	–
2MASSW J2258066+154416	M7.5	2800	6.0	2600	6.0	–	–	–	–	–	–	–	–
LP 412-31	M8.0	2500	5.5	2300	6.0	–	–	–	–	–	–	–	–
RG 0050−2722	M8.0	2300	4.5	2300	6.0	–	–	–	–	–	–	–	–
CTIO 0126575+280202	M8.5	2200	6.0	2200	6.0	–	–	–	–	–	–	–	–
TVLM 513	M8.5	2500	4.5	2600	5.5	–	–	–	–	–	–	–	–
LHS 2065	M9.0	2200	4.5	2200	6.0	–	–	–	–	–	–	–	–
TVLM 868	M9.0	2300	5.0	2200	6.0	–	–	–	–	–	–	–	–
PC 0025−010707	M9.5	2100	6.0	2200	6.0	–	–	–	–	–	–	–	–
2MASSW J0149090+295613	M9.5	2200	6.0	2100	6.0	–	–	–	–	–	–	–	–
2MASSW J0058425+065123	L0.0	2200	6.0	2200	6.0	–	–	–	–	–	–	–	–
2MASSI J0746425+200032	L0.5	2400	5.5	2300	6.0	–	–	–	–	–	–	–	–
2MASSW J1412244+163312	L0.5	2100	6.0	2100	6.0	–	–	–	–	–	–	–	–
2MASSW J0208183+254253	L1.0	2200	6.0	2100	6.0	–	–	–	–	–	–	–	–
2MASSW J1035245+250745	L1.0	2000	6.0	2100	6.0	–	–	–	–	–	–	–	–
2MASSW J0832045−012835	L1.5	2200	6.0	2200	6.0	–	–	–	–	–	–	–	–
2MASSW J1411175+393636	L1.5	2100	6.0	2100	6.0	–	–	–	–	–	–	–	–
2MASSW J0015447+351603	L2.0	2000	6.0	2000	6.0	–	–	–	–	–	–	–	–
2MASSI J0753321+291711	L2.0	1900	6.0	2000	6.0	–	–	–	–	–	–	–	–
2MASSW J0829066+145622	L2.0	2100	6.0	2000	6.0	–	–	–	–	–	–	–	–
2MASSI J1029216+162652	L2.5	2000	4.5	2000	6.0	–	–	–	–	–	–	–	–
2MASSI J0302012+135814	L3.0	1800	5.0	1900	5.5	–	–	–	–	–	–	–	–
2MASSI J0409095+210439	L3.0	1900	6.0	2000	6.0	–	–	–	–	–	–	–	–
2MASSW J0036159+182110	L3.5	2000	5.5	2100	6.0	–	–	–	–	–	–	–	–
2MASSW J1246467+402715	L4.0	1900	6.0	1800	5.0	(1700)	(5.5)	(1700)	(5.5)	–	–	–	–
2MASSW J0740096+321203	L4.5	1800	5.0	1900	6.0	(1700)	(5.5)	(1700)	(5.5)	–	–	–	–
2MASSW J1112257+354813	L4.5	1800	5.5	1900	6.0	(1700)	(5.5)	(1700)	(5.5)	–	–	–	–
2MASSW J0208236+273740	L5.0	(1900)	(6.0)	(1900)	(6.0)	1700	5.5	1700	5.5	–	–	–	–
2MASSW J1239272+551537	L5.0	(1800)	(5.5)	(1800)	(5.5)	1800	4.5	1700	5.5	–	–	–	–
2MASSI J0103320+193536	L6.0	–	–	–	–	1800	4.5	1600	4.5	–	–	–	–
2MASSI J0756252+124456	L6.0	–	–	–	–	1800	5.0	1500	5.5	–	–	–	–
2MASSW J0829570+265510	L6.5	–	–	–	–	1800	4.5	1800	4.5	–	–	–	–
2MASSW J0920122+351742	L6.5	–	–	–	–	1700	5.5	1700	5.5	–	–	–	–
2MASSI J0825196+211552	L7.5	–	–	–	–	1700	5.0	1700	5.5	–	–	–	–
2MASSW J0310599+164816	L8.0	–	–	–	–	1700	5.5	1600	5.0	–	–	–	–
2MASSW J1523226+301456	L8.0	–	–	–	–	1700	5.5	1600	5.0	–	–	–	–
SDSSp J083717.22−000018.3	T1.0	–	–	–	–	1500	5.5	1500	5.5	–	–	–	–
SDSSp J125453.90−012247.4	T2.0	–	–	–	–	1500	5.5	1500	5.5	(1900)	(4.5)	(2200)	(4.5)
SDSSp J102109.69−030420.1	T3.0	–	–	–	–	(2000)	(5.5)	(1500)	(5.0)	1400	5.0	1700	5.5
2MASSI J2254188+312349	T4.0	–	–	–	–	–	–	–	–	1300	5.5	1300	5.5
2MASSI J0755480+221218	T5.0	–	–	–	–	–	–	–	–	1400	5.5	1400	5.5
2MASSI J2339101+135230	T5.0	–	–	–	–	–	–	–	–	1200	5.5	1300	5.5
2MASSI J2356547−155310	T5.0	–	–	–	–	–	–	–	–	1200	5.5	1200	5.5
SDSSp J162414.37+002915.6	T6.0	–	–	–	–	–	–	–	–	1100	5.5	1200	5.5
2MASSI J0727182+171001	T7.0	–	–	–	–	–	–	–	–	1000	5.0	1200	5.0
Gliese 570D	T7.5	–	–	–	–	–	–	–	–	900	5.0	900	5.0
2MASSI J0415195−093506	T8.0	–	–	–	–	–	–	–	–	900	5.0	1000	5.0

extinction is essentially negligible (Fig. A.3 bottom panel). We note that a classification based on the reddening independent indices is less accurate than that done with the other indices in the case of no extinction (or perfect dereddening). The use of the reddening independent indices should be limited to the cases in which these indices are effectively needed because of uncertainties in the reddening towards the target sources.

Appendix B: Results and examples of model fits

We present in tabular format the results of the model atmosphere fits to the observed spectra. We also provide some examples of the details of the model fits and the χ^2 surfaces.

In Table B.1, we report for each star the best-fit model effective temperature and surface gravity for both the χ^2 and the

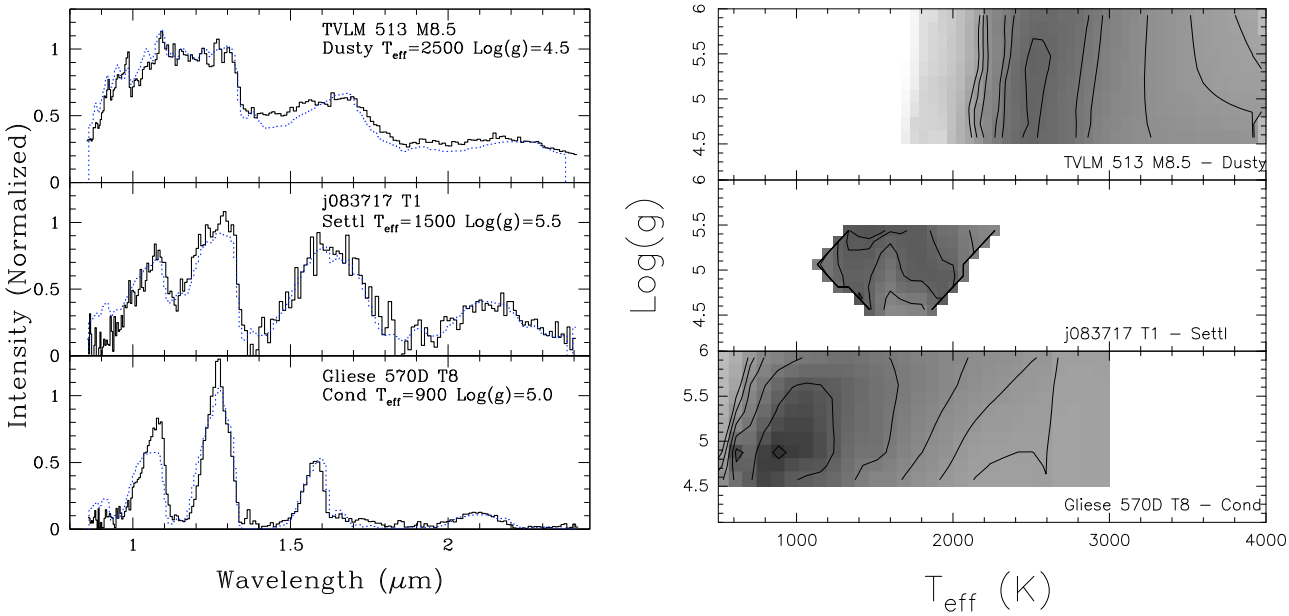

Fig. B.1. Examples of model atmosphere fits to our observed near-infrared spectra. *Left panel*: the observed spectra are shown as solid line, the best-fit model is shown as a dotted line. The names and spectral types of the dwarfs are marked together with the best-fit model atmosphere parameters. *Right panel*: χ^2 surfaces for a range of effective temperatures and surface gravities (dark regions correspond to lower values of the χ^2).

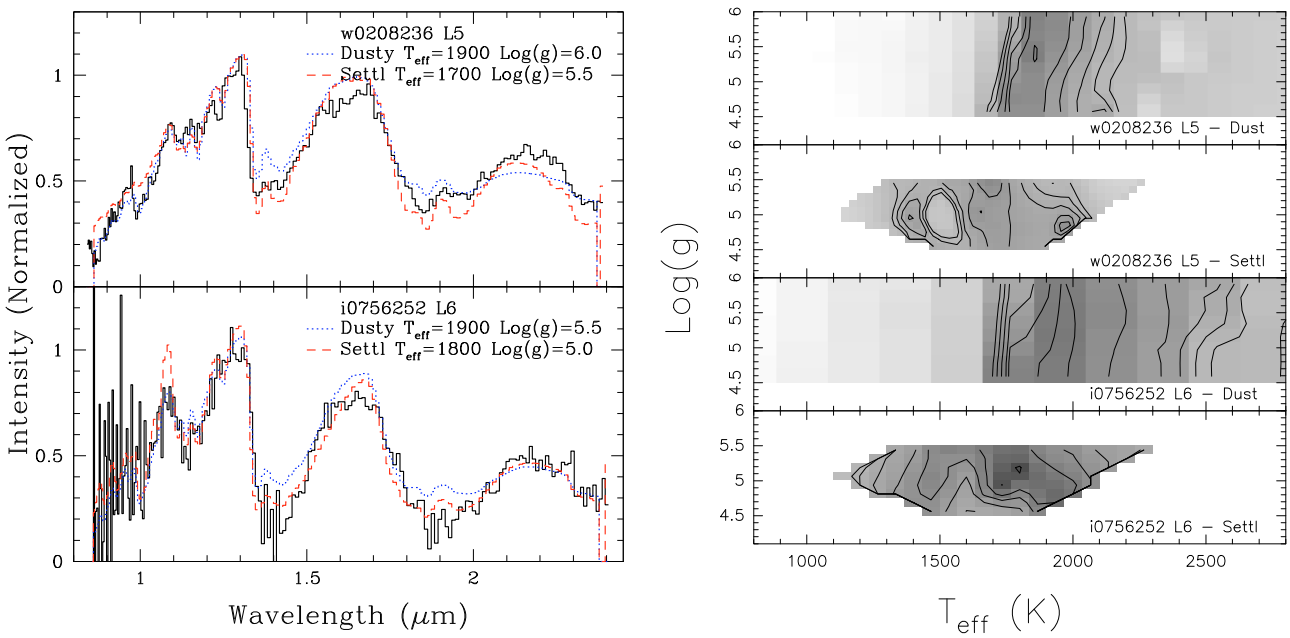

Fig. B.2. "Dusty" and "Settl" models fitted to an L5 and an L6 dwarf. *Left panel*: the observed spectrum is shown as a solid line, the "Dusty" models as dotted lines and the "Settl" models as dashed lines. The name of the dwarfs and the model parameters are marked on each panel. *Right panel*: χ^2 surfaces for each of the model fits as labelled.

q methods. The results are presented for the range of applicability of the various models. We also provide (in parentheses) the results of each class of models for objects one subclass beyond their range of applicability.

In Fig. B.1, we show the results of fitting the Lyon model atmospheres to the observations of dwarfs well within the range of applicability of the various models: "Dusty" models for an M 8.5 dwarf, "Settl" models for a T1 dwarf, and "Cond" models for a T8 dwarf. The fits derived with the χ^2 method are shown; as noted in Sect. 6, no major differences appear if the "q"-method is used. In the same figure, we also show the χ^2 surfaces for a grid of models spanning a suitable range of effective temperatures and surface gravities. We note that the effective temperature is more tightly constrained by these fits than the surface gravity. It is not the purpose here to discuss how well the models fit the observations and which observed features are more difficult to reproduce. A comprehensive discussion of these issues is provided in the series of papers by Allard et al. (2001), Leggett et al. (2001, 2002), and Cushing et al. (2008). What is useful to note is that our spectral library can also be a useful benchmark for identifying shortcomings in the models. As an example, the models cannot adequately fit the peak near 1.05 μm in the late T-dwarfs, while they provide an excellent fit throughout the remainder of the near-infrared domain.

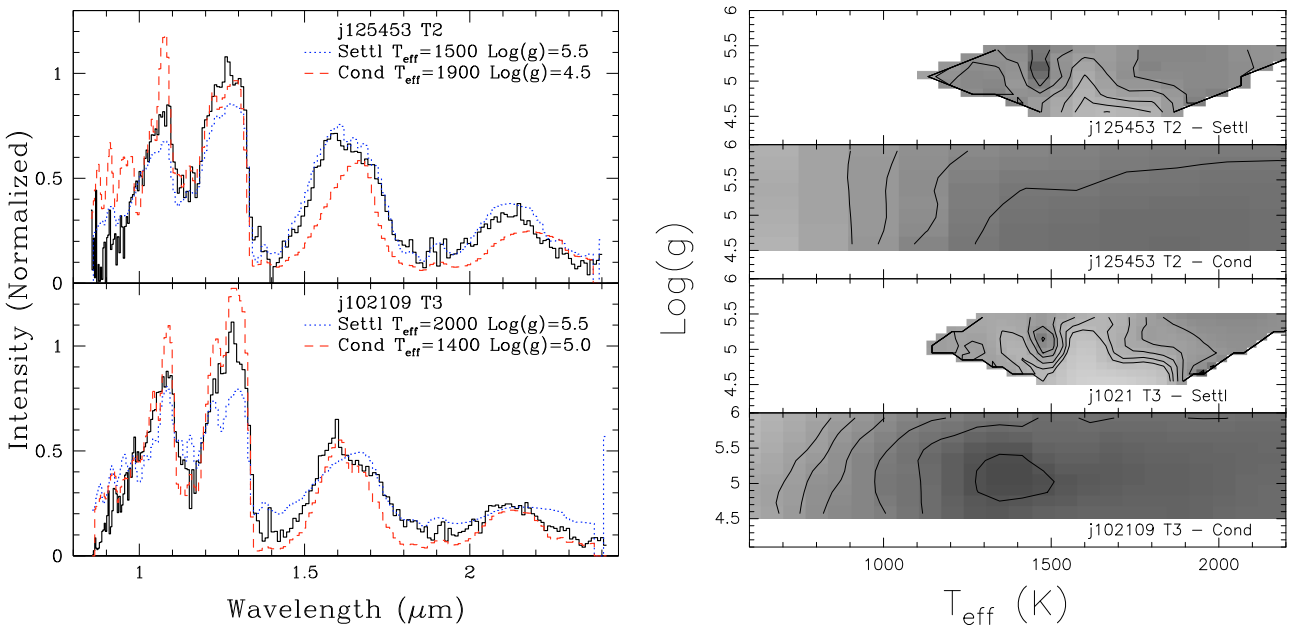

Fig. B.1. "Settl" and "Cond" models fitted to a T2 and a T3 dwarf. *Left panel*: the observed spectrum is shown as a solid line, the "Settl" models as dotted lines and the "Cond" models as dashed lines. The name of the dwarfs and the model parameters are marked on each panel. *Right panel*: χ^2 surfaces for each of the model fits as labelled.

In Figs. B.2 and B.1, we show examples of fits to dwarfs close to the transition of applicability of different classes of models. In these ranges, the different classes of models offer similar fits, each class with different types of shortcomings or successes. The model parameters, especially the effective temperature, do not differ significantly, except in the case of the T2 dwarf, where the "Cond" models offer a very poor fit to the observed spectrum.

References

Ackerman, A. S., & Marley, M. S. 2001, ApJ, 556, 872
Allard, F., Hauschildt, P. H., Alexander, D. R., Tamanai, A., & Schweitzer, A. 2001, ApJ, 556, 357
Allers, K. N., Jaffe, D. T., Luhman, K. L., et al. 2007, ApJ, 657, 511
Baffa, C., Gennari, S., Lisi, F., et al. 2000, in The Scientific Dedication of the Telescopio Nazionale Galileo, Conference held in Santa Cruz de La Palma on November 3–5, 2000
Baffa, C., Comoretto, G., Gennari, S., et al. 2001, A&A, 378, 722
Basri, G., Mohanty, S., Allard, F., et al. 2000, ApJ, 538, 363
Bouvier, J., Kendall, T., Meeus, G., et al. 2008, A&A, 481, 661
Burgasser, A. J. 2001, Ph.D. Thesis, California Institute of Technology
Burgasser, A. J. 2006, AJ, 134, 1330
Burgasser, A. J., Kirkpatrick, J. D., Cutri, R. M., et al. 2000, ApJ, 531, L57
Burgasser, A. J., Kirkpatrick, J. D., Brown, M. E., et al. 2002a, ApJ
Burgasser, A. J., Marley, M. S., Ackerman, A. S., et al. 2002b, ApJ, 571, L151
Burgasser, A. J., Kirkpatrick, J. D., Liebert, J., & Burrows, A. 2003, ApJ, 594, 510
Burgasser, A. J., McElwain, M. W., Kirkpatrick, J. D., et al. 2004, AJ, 127, 2856
Burgasser, A. J., Geballe, T. R., Leggett, S. K., Kirkpatrick, J. D., & Golimowski, D. A. 2007, ApJ, 637, 1067
Cardelli, J. A., Clayton, G. C., & Mathis, J. S. 1989, ApJ, 345, 245
Cruz, K. L., Burgasser, A. J., Reid, I. N., & Liebert, J. 2004, ApJ, 604, L61
Cushing, M. C., Rayner, T. J., & Vacca, W. D. 2005, ApJ, 623, 1115
Cushing, M. C., Marley, M. S., Saumon, D., et al. 2008, ApJ, 678, 1372
Delfosse, X., Tinney, C. G., Forveille, T., et al. 1997, A&A, 327, L25
Delorme, P., Delfosse, X., Albert, L., et al. 2008, A&A, 482, 961
Fan, X., Knapp, G. R., Strauss, M. A., et al. 2000, AJ, 119, 928
Geballe, T. R., Knapp, G. R., Leggett, S. K., et al. 2002, ApJ, 564, 466
Golimowski, D. A., Knapp, G. R., Strauss, M. A., et al. 2004, AJ, 127, 3516
Hunt, L. K., Mannucci, F., Testi, L., et al. 1998, AJ, 115, 2594
Henry, T. J., Kirkpatrick, J. D., & Simons, D. A. 1994, AJ, 108, 1437
Kirkpatrick, J. D., Henry, T. J., & Simons, D. A. 1995, AJ, 109, 797
Kirkpatrick, J. D., Reid, I. N., Liebert, J., et al. 1999, ApJ, 519, 802
Kirkpatrick, J. D., Reid, I. N., Liebert, J., et al. 2000, AJ, 120, 447
Kirkpatrick, J. D., Barman, T. S., Burgasser, A. J., et al. 2006, ApJ, 639, 1120
Leggett, S. K., Geballe, T. R., Fax, X., et al. 2000, ApJ, 536, L35
Leggett, S. K., Allard, F., Geballe, T. R., Hauschildt, P. H., & Schweitzer, A. 2001, ApJ, 548, 908
Leggett, S. K., Hauschildt, P. H., Allard, F., Geballe, T. R., & Baron, E. 2002, MNRAS, 332, 78
Lucas, P. W., Roche, P. F., Allard, F., & Hauschildt, P. H. 2001, MNRAS, 326, 695
Marley, M. S., Seager, S., Saumon, D., et al. 2002, ApJ, 568, 335
Martín, E. L., Delfosse, X., Basri, G., et al. 1999, AJ, 118, 2466
Nakajima, T., Oppenheimer, B. R., Kulkarni, S. R., et al. 1995, Nature, 378, 463
Nakajima, T., Tsuji, T., & Yanagisawa, K. 2004, ApJ, 607, 499
Natta, A., Testi, L., Comerón, F., et al. 2002, A&A, 393, 597
Oliva, E. 2003, Mem. Sc. Astr. It., 74, 118
Rebolo, R., Zapatero-Osorio, M. R., & Martín, E. 1995, Nature, 377, 129
Reid, I. N., Burgasser, A. J., Cruz, K. L., Kirkpatrick, J. D., & Gizis, J. E. 2001, AJ, 121, 1710
Strauss, M. A., Fan, X., Gunn, J. E., et al. 1999, ApJ, 522, L61
Testi, L., D'Antona, F., Ghinassi, F., et al. 2001, ApJ, 552, L147 (T01)
Testi, L., Natta, A., Oliva, E., et al. 2002, ApJ, 571, L155
Tinney, C. G., Delfosse, X., Forveille, T., & Allard, F. 1998, A&A, 338, 1066
Tokunaga, A., & Kobayashi, N. 1999, AJ, 117, 1010
Tsuji, T. 2002, ApJ, 575, 264
Tsuji, T., Nakajima, T., & Yanagisawa, K. 2004, ApJ, 607, 511
Warren, S. J., Mortlock, D. J., Leggett, S. K., et al. 2007, MNRAS, 381, 1400
Wilking, B. A., Greene, T. P., & Meyer, M. R. 1999, AJ, 117, 469
Wilking, B. A., Mikhail, A., Carlson, G., Meyer, M. R., & Greene, T. P. 2003, in Brown Dwarfs, ed. E. L. Martín, IAU Symp., 211, 97